Teaching Machines to Measure Economic Activities from Satellite Images: Challenges and Solutions

Donghyun Ahn[1], Meeyoung Cha[1,2], Sungwon Han[1],
Jihee Kim[3], Susang Lee[3], Sangyoon Park[4],
Sungwon Park[1], Hyunjoo Yang[5], and Jeasurk Yang[6]

[1]School of Computing, KAIST
[2]Data Science Group, Institute for Basic Science
[3]College of Business, KAIST
[4]Faculty of Business and Economics, University of Hong Kong
[5]School of Economics, Sogang University
[6]Department of Geography, National University of Singapore

June 15, 2020

Abstract

How can we teach machines to quantify economic activities from satellite images? In this paper, we share the research progress in answering the question. We document what we have learned so far – characteristics of geospatial data including satellite images and recent developments in computer vision and image processing. We then identify some challenges in adopting the machine learning techniques to address the question. We present two of our proposed deep learning models that address some of the challenges: the first model predicts economic indicators from a satellite image by resolving the mismatch in data representation, and the second model learns to score the level of economic development of a satellite image even without ground-truth data. We also talk about our future research agenda to improve the models and to apply them for economic research and policy-making in practice.

Keywords: Machine Learning, Satellite Imagery, Measurement of Economic Development

JEL Codes: C82, O11, O18, O57

1. Introduction

Artificial intelligence (AI) and machine learning are transforming every nook and corner of our world. In recent years, we have seen the emergence of calls for applying AI and machine learning to solve socioeconomic, humanitarian, and environmental problems from both the profit and nonprofit sectors. For example, in 2018, Google's AI for Social Good hosted the AI Impact Challenge, which awarded 25 million US dollars to socially beneficial projects and organizations tackling global challenges (Google, n.d.). Likewise, Microsoft, another tech giant, has launched a series of AI for Good initiatives for empowering AI-equipped organizations to bring positive impacts via a pledge of 165-million-dollar financial support (Microsoft, n.d.). From the nonprofit side, the United Nations (UN) has been advocating the promising role that AI can play to achieve sustainable development goals through their annual AI summit (Butler, 2017). According to a report by McKinsey Global Institute (Chui et al., 2018), there are approximately 160 AI applications for social good, and they cover all 17 agendas for sustainable development set by the UN.

Among many applications of AI, the combination of computer vision and spatial data have made remarkable advancement and shared the spotlight from both researchers and practitioners. The growing applications of spatial data, such as maps and satellite images on socioeconomic problems, can attribute to the technical breakthrough in geographic information systems (GIS) and machine learning based on massive computing power. Equally important has been the massive amount of data provision from both the public and private sectors. Indeed, once generated and preprocessed for third-party access, large-scale data have become readily available in almost real-time. Moreover, with the assistance of crowdsourcing, big spatial data have been attached to a variety of labels, changing many knotty problems to be solvable and an essential component of training and evaluating supervised machine learning. Naik et al. (2017) employed a computer vision method to the time-series street-view images with crowd-

sourced safety ratings to examine the physical dynamics of cities. High-resolution satellite imagery, another primary source of spatial data, has been exploited in a convolutional neural network to predict consumption and wealth at the local level (Jean et al., 2016; Yeh et al., 2020).

This paper presents how economists can integrate machine learning techniques into satellite images to unearth economic measures more effectively from the view above and to devise better economic policies. We first glance at how satellite imagery has contributed to unraveling the traditional economics problems and will expand its potential with the aid of machine learning in complementing the economics literature. In particular, daytime, rather than nighttime, satellite imagery with high resolution is our focus here. Subsequently, we introduce the current availability of both satellite imagery and geographic ground-truth data. We also review the recent developments in computer vision and image processing that can be of potential use in utilizing satellite images and economic data. We then identify some of the challenges in teaching machines with satellite images as inputs and economic indicators as outputs: (1) defining economic labels, (2) data labeling to construct ground-truth, (3) lack of available ground-truth economic data, (4) mismatch between district-level economic data and grid-level satellite image data, (5) overfitting problem, (6) generalizability problem, and (7) Black Box problem. Adding higher value is our suggested approach to these difficulties and potential avenues for satellite imagery combined with machine learning in future research.

Satellite Data for Economic Research

Satellite imagery has never been so welcomed among the economics literature. Owing to the recent development of computer vision algorithms, economists are collecting big satellite data not just to explore novel questions but also to tackle questions that could not be answered with traditional data sources. A comprehensive survey by Donaldson and Storeygard (2016) has lowered the technical barrier to entry by providing a gentle introduction to satellite data for economists and its applications. Over the past two

decades, however, satellite data sources utilized in much literature has mainly been either luminosity from nighttime satellite images (i.e., night lights) or sensory data for special purposes (e.g., ecological, meteorological, or topographical studies; for review, see Donaldson and Storeygard 2016). Besides, despite the extensive coverage in both time and space, prior studies often focused on a single country or area of interest only at certain times.

Nighttime Satellite Imagery as a Proxy for Economic Activity and Its Limitations

Nighttime satellite images or night lights are now a prominent, plausible proxy for global and local economic activity; They have proven their versatility and robustness in the economics literature. Gathered by US Defense Meteorological Satellite Program's Operational Linescan System (DMSP-OLS) and distributed by NOAA National Geophysical Data Center, luminosity data are represented as a six-digit digital number (DN) between 0 and 63 at a grid level; the higher the DN, the brighter the light radiance.

Since the pioneering works by Chen and Nordhaus (2011) and Henderson et al. (2012), night lights began to gain the attention and became a mainstream measure of economic output, widely applied in a multitude of development economics research (for review, see Michalopoulos and Papaioannou 2018). Recent papers have exploited and verified the strong correlation between light density and output statistics at the regional/within-country as well as global/cross-country levels (Chen and Nordhaus, 2011; Henderson et al., 2012; Pinkovskiy, 2017; Pinkovskiy and Sala-i Martin, 2016). In addition to economic production, nighttime satellite imagery has been used to predict energy consumption (Xie and Weng, 2016), epidemic fluctuations (Bharti et al., 2011), regional favoritism (Hodler and Raschky, 2014; Lee, 2018), and urban growth in developing countries (Dingel et al., 2019; Michalopoulos and Papaioannou, 2013; Storeygard, 2016), even in areas without or lacking the reliable traditional measures.

While night lights can be advantageous in measurement objectivity and wide spatial and time-series coverage, they bare some drawbacks. Michalopoulos and Papaioannou (2018) discuss several caveats of using luminosity at nighttime. The two most notable

shortcomings are blooming and saturation. Blooming refers to the magnified light emission from one pixel to adjacent pixels due to its reflection over some types (e.g., water- or snow-covered) of terrain. Saturation pertains to the top- or bottom-censored values of DNs resulting from amplification for detecting highly bright or dim lights. Because of these limitations, luminosity at night exhibits underperformance in areas at the extreme ends of the wealth or income spectrum. Using relatively recent data from the Visible Infrared Imaging Radiometer Suite (VIIRS), instead of DMSP-OLS, can alleviate the blooming and saturation effects a little (Baragwanath et al., 2019). An alternative solution to these limitations is the use of radiance-calibrated luminosity data (e.g., Henderson et al., 2018).

Advantages of Using Daytime Satellite Imagery and Applications in Economics High-resolution daytime satellite imagery presents a raw picture of the world at a fine-grained level, from which measures of human activities can be extracted directly. Daytime satellite images are capable of capturing and offering more lavish features and patterns observable from above compared to nighttime images. Although the accessibility to high-resolution daytime satellite imagery goes way back, its frequent appearance in the literature has only recently become possible due to the analytical complexity resulting from high dimensions and lack of structures (Donaldson and Storeygard, 2016). Thus, daytime satellite images at high resolution began to be utilized by leveraging the high representation power of deep learning architectures.

One popular usage of daytime satellite imagery is the land cover classification. Jayachandran et al. (2017) classified daytime images from QuickBird, a commercial satellite with high-resolution support, and assessed the impact of Payments for Ecosystem Services on (de)forestation in Ugandan villages. Similarly, Baragwanath et al. (2019) detected urban markets by examining land covers from three different daytime satellite datasets–including MODIS, GHSL, and MIX–based on supervised learning. Like the night light examples, daytime luminosity can also be a unique proxy for socioeconomic welfare, as shown in the recent study of Marx et al. (2019) on ethnic patronage among

informal settlements in Kenya.

Notable advancement was made by Jean et al. (2016), who predicted poverty across five African nations via a multi-stage approach called transfer learning. In their work, transfer learning first trained a machine first to compare nighttime luminosity with daytime pictures and then predicted consumption and wealth from daytime features with the actual survey data. To the latest, Yeh et al. (2020) added more value to Jean et al.'s (2016) finding by outperforming the extant model with analogous technique and using only publicly available satellite data. One significant contribution that parallels our attempts to be illustrated in later parts is their use of scarce labeled data, which often hinders such prediction tasks.

The remainder of the paper has the following structure: In Section 2., we discuss the characteristics of geospatial data including satellite imagery and provide some accessible sources in detail. In Section 3., we review the recent developments in computer vision and image processing that can be applied to satellite images, and discuss several challenges in using satellite images to teach machines to extract economic information captured in satellite images. Section 4. describes our efforts to develop machine learning techniques that use daytime satellite images to measure economic development. We also share our future research agenda and conclude in Section 5.

2. Geospatial Data for Economic Research

2.1. Satellite Imagery Data

The combined methods of machine learning and remote sensing highly depend on satellite images. Satellite imagery datasets are stored in Raster formats, which are sets of a large number of grid cells (or pixels) with corresponding values and geographic coordinates. Satellite imagery datasets can be classified by diverse characteristics: orbits of satellite, resolution, and the numbers of spectral bands. Imagery is taken by two-orbit satellites; geostationary satellites have orbits to continuously take images of a

fixed point, while sun-synchronous satellites have nearly polar orbits to keep the same relational position with the Sun to capture any points of Earth.

The Resolution of Satellite Imagery

The resolution of satellite images is described as a meter per pixel; however, as machine learning techniques often use split individual images for analysis (e.g. (Jean et al., 2016)), it is described with zoom level resolution in the field. Zoom level coordinate system is based on how many 256-pixel wide tiles are used to divide the whole world. As the system uses individual tiles, it is useful as input in deep learning models. Given that zoom level 0 uses one tile to show the whole world, the tiles are split into four when a zoom level goes up. The resolution of zoom level 15 is 4.773m per pixel, 16 for 2.387m, and 17 for 1.193m. A popular example of the system is the Google Maps service. The high-resolution satellite images (at most 5m resolution) are mostly used as daytime imagery input in machine learning fields for predicting economic variables.

The Spectral Bands of Satellite Imagery

Satellite sensors catch all wavelengths of the electromagnetic spectrum differently. Thus, individually recorded wavelengths are referred to as spectral bands, and the number of bands varies depending on the sensors. The bands include not only visible lights of Red, Blue, and Green, but also other bands such as coastal aerosol, near-infrared (NIR), water vapor, short-wave infrared (SWIR), and others. The combination of bands can detect numerous types of human and natural objects; for example, Normalized Difference Vegetation Index (NDVI) calculated by Red and NIR bands can measure the state of plant health. However, machine learning studies to date tend to focus on Red, Blue, and Green bands.

The Cost of Satellite Imagery

The cost of satellite images depends on the resolution and size of the area. The high-resolution datasets cost significantly up to USD 30/km^2; selected examples of images are Worldview 3/4 (30cm resolution), GeoEye 1 (40cm), KOMPSAT-3A (55cm), Quick-

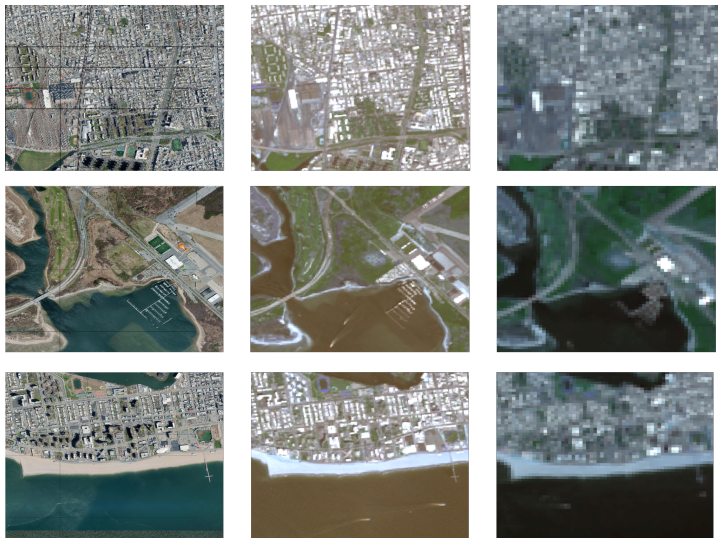

Figure 1: Publicly Available Satellite image, Brooklyn, NY.

Note: World Imagery (left), Sentinel2 (middle), Landsat8 (right)

bird (60cm), KOMPSAT 2 (1m), and SPOT 6/7 (1.5m). On the other hand, there are publicly available datasets, including Landsat series (from 30m to 80m), Sentinel 2 (10m), and World Imagery (on average up to 1.2m) via the REST APIs of Esri®ArcGIS (Johnston et al., 2001). Landsat series are available from 1972, Sentinel 2 from 2015, and World Imagery for the only one-time snapshot.

2.2. Grid-level Ground-truth Data

For estimating economics with machine learning, it needs ground-truth data for training and evaluating the models. The primary approach is to use official district-level socioeconomic statistics as ground-truth (Jean et al., 2016). In this approach, the worldwide provided datasets such as Demographic and Health Surveys (DHS), are useful for analyzing developing countries. However, district-level data have caveats as requiring other grid-level supplementary data (e.g., nightlight data) corresponding to split individual satellite images.

Grid-level Ground-Truth Data Used to Date

Thus, there come various attempts to use grid-level data in recent studies. Hardly do datasets provide official socioeconomic statistics at the grid level; raster datasets are alternatively used to split into grids. Nightlight data is widely utilized (Jean et al., 2016). Moreover, Han et al. (2020a) used Facebook humanitarian data for grid-level prediction of population. Facebook has contributed by making the most precise population map of the world, covering most of the Asian and African countries Facebook (2020). The estimation is at the resolution of an arcsecond-by-arcsecond scale. Online geocoded data, such as georeferenced Wikipedia articles, have also been used as proxies for socioeconomic statistics (Fatehkia et al., 2018; Sheehan et al., 2019; Uzkent et al., 2019; Rama et al., 2020).

Other Possible Ground-Truth Data

There are several other possible grid-level data for proxies of economic activities. First, among many digital elevation data, the Normalized Digital Surface Model (NDSM) is useful in detecting human development at the grid level. Calculated by Digital Surface Model (DSM) and Digital Terrain Model (DTM), NDSM displays the height of objects over the surface. Thus, NDSM can show a total volume of human-constructed artificial objects in a given area. However, since digital elevation datasets are relatively expensive, similar types of data, such as building footprint data, can be used as an alternative. The building footprint data provide geospatial shapes of all buildings. It is often provided by selected countries and publicly available from Openstreetmap data (OSM). If footprint data is multiplied by floor levels of each building, it is the gross floor area and similar to NDSM in concept. Third, the land use and land cover (LULC) data describes the feature types of land, including vegetation, water, built-up, and others. LULC can capture economic activities such as urbanization (built-up) or agriculture (vegetation). LULC is diverse in terms of providers and class categories based on geographical and national contexts, but there is also global-scale data such as Copernicus Global Land Cover. Lastly, the land surface temperature (LST) describes the radiative skin temperature of the land surface at day and night. Wang et al. (2018)

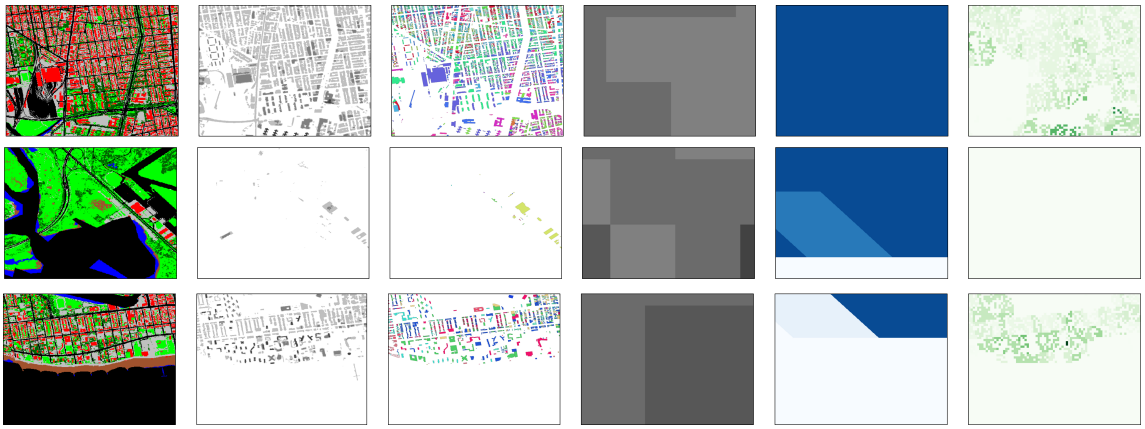

Figure 2: Examples of Grid-level Ground Truth Data, Brooklyn, NY.

Note: From left, (1) Landuse/landcover classification (NYC opendata), (2) NDSM (Digitalglobe), (3) Building footprints(NYC opendata), (4) Nightlight data (NOAA), (5) Land surface temperature (MODIS), (6) Facebook population data.

posed that patterns of LULC might have potential impacts on LST; the city core had higher nighttime LST than rural areas, especially in cold seasons. LST data is publicly available from MODIS.

2.3. Reviews from a Data Perspective

The previous two sections examined satellite imagery and hyperlocal-level ground truth data used in the field of machine learning in economics and remote sensing. However, there are several caveats with utilizing the data. The predominant limit and tendency of the previous approaches are to focus on high-resolution satellite images instead of low and publicly available ones. As a result, few pieces of research have been conducted on time-series analysis due to high costs. Moreover, the applicability of the study is low in that the method to date cannot be easily followed. Although Yeh et al. (2020) posed the possibility of using the public source, it is urgent to develop other machine learning models for economic prediction with publicly available imagery with multi-temporal data; Sentinel2 could be appropriate with a 10m resolution source from 2015. Second, the satellite images cannot be interchangeably mix-used because they differ from each other in terms of resolution, data type, color tones, degree of correction, the numbers

of bands, coordinates, and other geographical metadata. This reduces the applicability of models in which performance becomes lower with other sources of satellite imagery. Third, as literature has been based on split individual tiles, the analysis inevitably takes a great effort and time to clip massive raster data into smaller tiles. Although the World Imagery dataset offers a clipped version of image tiles for users, other datasets need to be split with tile extents. Lastly, there is no consensus on which hyperlocal or grid-level data, beyond district-level statistics, should be used for ground truth of economic activities. Research is needed to determine the most explanatory information among various data sources suggested in the previous section.

3. Challenges in Teaching Machines to Read the Economic Context of Satellite Images

3.1. Machine Learning for Satellite Image Processing

We have seen remarkable progress in teaching machines to recognize objects in an image over the last decade. Machine learning models in computer vision and image processing require a massive data set to train and test, and thereby enormous amounts of computing power to process the data. Lack of such data had been the major hurdle, but ImageNet (Deng et al., 2009), the large-scale crowdsourced data of labeled images, sparked the fast growth of the technology. ImageNet has over 14 million images that are organized according to nouns in the WordNet, a lexical database with the hierarchical structure. With ImageNet, machines can be trained to learn what cats look like and to distinguish them from other animals. The ImageNet Large Scale Visual Recognition Challenge also has played a crucial role in serving as an incentive for researchers. The state-of-the-art method as of May 2020 shows the top 5 accuracy rate of 98.7% – it is only 1.3% of the time that machines' top 5 guesses for the name of an object in

a presented image do not hit the right answer.[1] This beats average humans as the corresponding rate is about 95% for humans.

Generally speaking, object recognition can be divided into two tasks: object localization and object classification. Object localization is to find a specific area, represented as a bounding box, in an image where an object resides. Object classification is to find a label for an object in an image. Object detection is then the combination of the two: detect an area where a specific object is contained and figure out the label for the object.

Object detection techniques to detect semantic instances, such as airplanes or cars, have been widely applied to analyze satellite imagery (Wang et al., 2020; Chen et al., 2014; Guo et al., 2018). In many cases, convolutional neural networks (CNN), a deep-learning neural network algorithm, are first trained for object classification, and then they are trained to draw a bounding box with ground-truth boundary data, where boundaries are marked by human annotation (See Figure 3) (Guo et al., 2018).

Figure 3: Object Detection in Satellite Images

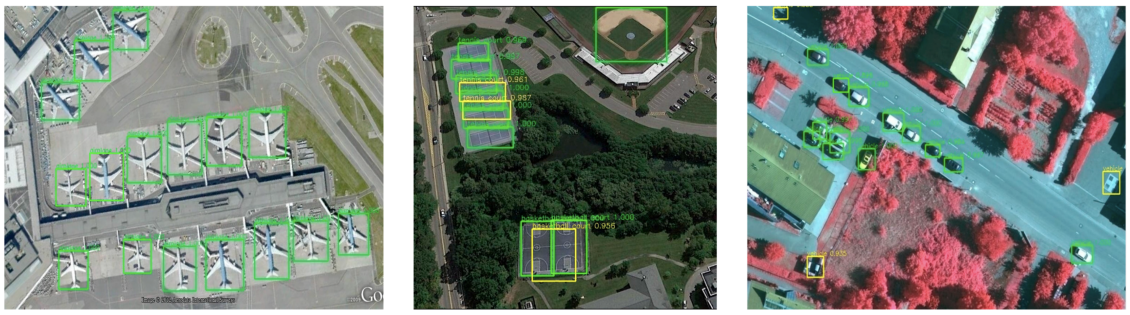

Source: Guo et al. (2018)

While object localization and image classification can be regarded as basic techniques, there are many other techniques in computer vision and image processing that can be applied to analyze satellite images. Instead of object localization, which

[1] https://paperswithcode.com/sota/image-classification-on-imagenet reports the most up-to-date results.

Figure 4: Satellite Image Data for Change Detection

(a) Rio on Apr 24, 2016 (b) Rio on Oct 11, 2017 (c) Ground-truth Change

Source: Daudt et al. (2018)

Note: The ground-truth change is annotated by humans.

draws bounding boxes, we may want to figure out the exact boundaries (or edges or contours) of an object or some spatial instance. Or, one can take a pixel-based approach, such as in image segmentation. In image segmentation techniques, an image is first partitioned into multiple semantic segments to generate sets of pixels with similar characteristics. The algorithms then put a label on each set of pixels. In the end, every pixel in an image will have a label (Chen et al., 2018). If the pixel level constructs LULC data, it can be used to test the performance of image segmentation models. At the same time, LULC data can be created by applying image segmentation.

As many economics questions involve growth or changes over time, detecting temporal changes in satellite images can be of potential interest. What is essential in developing a change detection method is to define a change that we want to measure and collect training data for such changes. Figure 4 shows an example of such data. Change detection techniques were designed to detect the movement of buildings or changes in terrain (Daudt et al., 2018) or to detect the long-term changes in the forest, while ignoring other temporary changes such as clouds or other weather conditions (Khan et al., 2017). These deep learning-based approaches either make a difference in high-level features coming out of CNN layers, or train a CNN model using two images to compare as input, and changes annotated by humans or administrative data as output.

3.2. Challenges

While processing images to identify objects in them has been successful, processing satellite images and uncovering their economic information poses different challenges.

Defining Economic Labels

First of all, we do not yet have ImageNet for satellite imagery and economic information: while we have abundant satellite image data, we don't have a set of economic labels that are readily available. To apply the currently available object recognition algorithms, we need to explicitly figure out what to teach: the ground truth for economic information by grid-level. Once the ground-truth data is available, we can teach machines that geographic characteristics captured in a satellite image are linked to the given economic information.

The first step is then to define classes of labels, which represent economic information that can be captured in satellite images. With the defined economic labels and satellite images, we can formulate a classification machine learning problem. What could be the economic version of WordNet for satellite images? Objects that can be observed from satellite imagery, such as buildings, roads, airplanes, cars, and so forth, can serve as a class of labels. LULC and crop/vegetation categories can also provide a set of label classes. Taking an urban development perspective, 'urban/rural/uninhabited' labels can be helpful. Considering production side of an economy, 'agriculture/manufacturing/service/residential' classification can also do a job. For each of these classifications, we may want to introduce a deeper hierarchy. For example, we can classify further 'urban'-labeled images with 'super-urban/urban/suburb.' With these classifications, we can design a deep learning classification algorithm to assign a label to each satellite image.

Data Labeling to Construct Ground-truth Labels

The next step is to put a label to each satellite image, which requires human annotation. However, annotation can be costly in both time and money due to the massive size of satellite images and labeled data required to train and test. Therefore, many projects

such as SpaceNet Challenges[2] or Openstreetmap take a crowdsourced approach in collecting labeled data. When adopting crowdsourcing, a design of labelling tasks for efficiency and data validation for labeled data quality can be challenging.

Lack of Available Ground-truth Economic Data

While addressing the classification problem can be useful, what is more relevant for economic research is to put a number to each satellite image, which can be a measure of economic activities such as population, consumption, wealth, inequality, poverty, etc. This comes down to a regression task in machine learning with satellite images. For example, we may want a machine learning algorithm to predict poverty from the satellite images of a particular region.

For this prediction task, economic statistics or administrative data at the grid-level is required as the ground-truth to train and test the algorithm. The biggest challenge is then the availability of such ground-truth economic data needed for cross-sectional and time-series analysis. One solution we propose in Section 4.2.that can be applied under absence of ground-truth data is redefining the task to predict *relative* economic measures not absolute measures. We develop a deep learning technique which makes use of economic labels and requires only lightweight human annotation to compare different clusters of satellite images given some economic criteria. Our approach adopts metric learning after classification and clustering tasks.

Mismatch between District-level Economic Data and Grid-level Satellite Image Data

While economic data is usually available by the administrative unit, satellite images are stored in a grid format. This mismatch in representation makes existing models not applicable to satellite images and district-level ground-truth: a district can be of any polygon shape spreading over multiple satellite image tiles, which changes the input dimension (the number of satellite images of the district) to the algorithm every time.

[2]https://spacenet.ai/

In Section 4.1., we propose a deep learning model to learn sophisticated spatial features of an arbitrarily shaped district based on high-resolution satellite images to produce a fixed-length representation of economic measures.

Overfitting Problem

When the size of labeled data is not big enough, a deep learning model may fit too closely or too exactly to a particular training dataset, which is referred to as the overfitting problem. Overfitting leads models to lose generalizability and become less applicable to other datasets. The lack of available ground-truth economic data and mismatch in representation, the previously discussed problems, make the overfitting problem highly relevant in our context.

Generalizability Problem

Since some of geographic characteristics can be unique for each continent or for each country, designing a deep learning technique that are generally applicable is a difficult challenge. Moreover, some geospatial features contained in a satellite image can be affected by when the image was recorded, which aggravates the problem. There are two approaches we can take: either to develop a model that can transfer knowledge between different regions or to optimize a model for each region. We plan to test and expand generalizability as much as possible in developing deep learning models.

Black Box Problem

AI models, including deep learning, are criticized that prediction results from the models are not interpretable or explainable, so called as *Black Box problem* of AI(Castelvecchi, 2016). The lack of interpretability and explainability prevents wider use of machine learning algorithms both in social science research and in practice despite its advantages. Making a model more interpretable and explainable is regarded as the most important and pressing challenge in the current literature. In our model presented in Section 4.2., we utilize some interpretable input to help explain the prediction result, which we believe one step towards tackling the problem.

4. Our Progress

In this section, we introduce our technical approach to solve some of the challenges discussed in the previous section—mismatch in data representation and lack of available ground-truth economic data.

4.1. Matching Grid-level Satellite Image Data to District-level Economic Data[3]

The existing machine-learning models are not applicable for predicting district-level data. Since districts, unlike grids, can be of any polygon shape, this trait leads to a mismatch when attempting to use satellite images with deep learning-based approaches. TO overcome this, we propose a model that efficiently extract key fixed-length features from any number of satellite images from an arbitrary region. Our method, called Representation Extraction over an Arbitrary District (READ), utilizes daytime satellite image tiles whose three vertices belong entirely to the polygon representing each district. A single district can contain vastly different land covers such as urban built-up, water, forest, etc. Our task is to learn these sophisticated spatial features of an arbitrarily shaped district based on high-resolution satellite images to produce a fixed-length representation of economic measures.

READ is a lightweight method of measuring economic activities from high-resolution images. The learned features are robust to the size of the original labels, such as population density, age, education, income, etc. We present a comprehensive evaluation of the model based on a rich set of data from a developed country, South Korea, and demonstrate its potential use in a developing country, Vietnam. The overall architecture of READ is illustrated in Figure 5.[4]

[3]This subsection is adapted from our work Han et al. (2020a).
[4]The code is released at GitHub. https://github.com/Sungwon-Han/READ

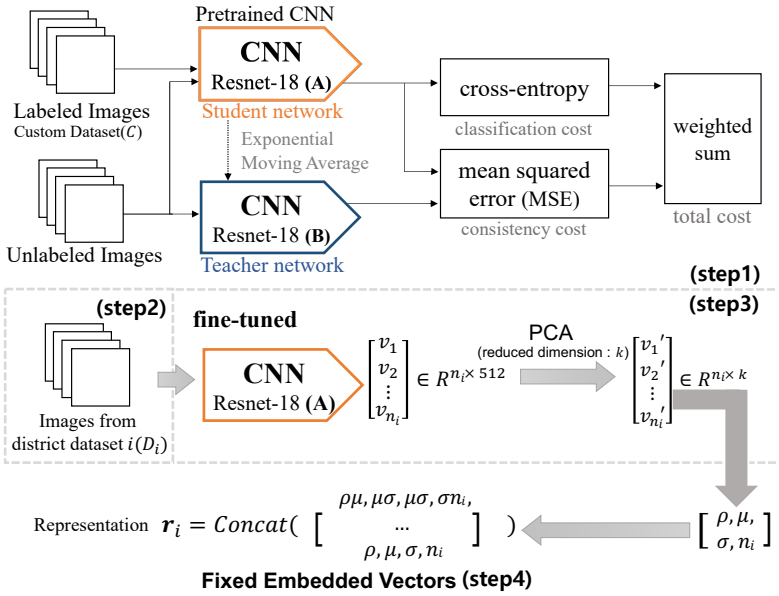

Figure 5: Overview of READ Model

Note: Our model operates in four steps: (Step-1) training embedding via semi-supervised learning and transfer learning, (Step-2) Data Pruning, (Step-3) dimensionality reduction, and (Step-4) calculating the embedded spatial statistics and conducting regression for validation.

4.1.1. Model

We first state the problem. Let d_j^i be the j-th satellite imagery of district $i \in U$, where U is the complete set of districts in a country. Let D_i be the set of satellite imagery of district i. Since districts can be of any shape and size, the number of satellite images in D_i varies from one district to another. We define this number for district i as n_i, i.e., $d_j^i \in D_i$ where $1 \leq j \leq n_i$. Then, the main problem is defined as follows:

> **Problem definition:** Given an image set D_i of district i, can we extract fixed-sized (s) representations $\mathbf{r}_i$ (i.e., $\mathbf{r}_i \in \mathbf{R}^s$ of any district i) and predict y_i the attribute of interest in the district i?

Embedding Training via Semi-supervised Learning

Network learning with supervision was used to extract meaningful information, so-called embeddings, from satellite imagery. Embedding is the learned representation of

a given input, and it can be extracted from network's hidden layer. To train the network with its embeddings, we constructed a labeled custom dataset ($\mathcal{C}$) that includes 1,000 randomly selected satellite images and employed the following three labels directly related to a degree of urbanization: urban, rural, and uninhabited. We hired four annotators to obtain the labels of the images. We integrated all annotators' decisions as soft labels (i.e., average votes), which were then used to build a classifier that divides satellite images into three classes. However, obtaining reliable labels for each satellite image tile was a time-consuming task. Here, a key challenge was the relatively small number of labeled data, which was addressed by adapting a semi-supervised learning approach.

Semi-supervised learning aims at training classifiers based on a small amount of labeled data and a large amount of unlabeled data. Mean Teacher (Tarvainen and Valpola, 2017), which is a powerful model in this domain, utilizes unlabeled data to penalize predictions that are inconsistent between the student and teacher models. This regularization technique can provide smoothing in the decision boundary for a robust and accurate forecast. We used the Mean Teacher architecture with the ResNet18 backbone for training. In addition to semi-supervised learning, we concurrently adopted transfer learning. Transfer learning is a learning technique that utilizes knowledge from another dataset to solve the main task. Knowledge gained from a similar dataset helps efficient training and prevents the model from overfitting. Following the idea, we first pretrained the CNN model with the ImageNet dataset (Deng et al., 2009), and then use the pretrained model as an initial student network in the Mean Teacher model.

To determine whether the trained classifier extracts essential features, we visualized sample images into three-dimensional space by reducing the embedded vectors by PCA. Figure 6 displays the extracted features in the reduced vector space of sample images of various urban and rural areas. Here, the rural and urban images are separated and aligned well in the virtual direction (i.e., red and blue arrows). Furthermore, these virtual axes represent the degree of urbanization. The left-hand side of the picture

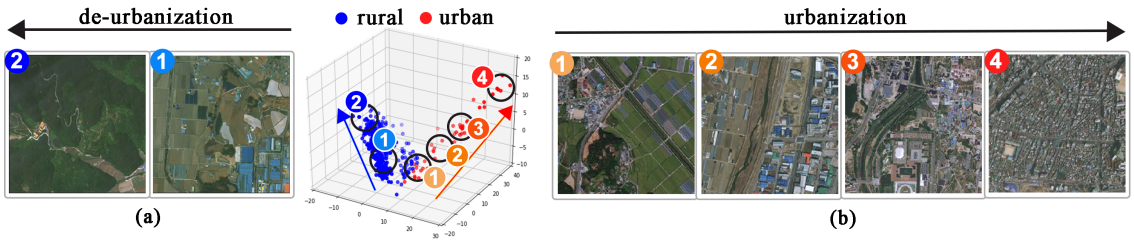

Figure 6: Graphical Representation of an Embedded Space: Urban vs. Rural

Note: This embedded space analysis shows that rural images (blue) are well separated from more urban images (red). For the blue cluster, as we observe images from anchor points 1 to 2, the de-urbanization trend becomes more pronounced. In contrast, for the red cluster, as we observe images from anchor points 1 to 4, the degree of urbanization becomes more intense.

shows two satellite image tiles. Both tiles have rural characteristics, and the images that seem to contain a smaller human population are positioned further toward the blue arrow (i.e., tile "2" seems less urbanized than tile "1"). The image tiles on the right-hand side contain capture more populated areas. Tiles "3" and "4" that are toward the end of the red arrow show a highly urbanized cityscape, whereas tiles "1" and "2" contain fewer residential areas. This figure demonstrates the strength of our model in its ability to learn high-level features and align satellite images along these virtual axes.

Data Pruning

According to the Global Rural-Urban Mapping Project, only 3% of the land cover is an urban area, and approximately 40% of the land is an agricultural area (Doxsey-Whitfield et al., 2015; Foley et al., 2005). The remaining uninhabited area accounts for the most considerable portion of the earth. Since such regions do not show human artifacts, they could act as noise when extracting representations related to human activities. We built a CNN classifier by filtering areas that are probably uninhabited. For the training, we reused a custom dataset that included 1,000 randomly selected satellite images. Of the initial 96,131 images, 51,618 (53.702%) images were removed in this manner.

Dimensionality Reduction of Embedding

The next step reduces the dimensions from the final layer in ResNet18 into smaller sizes. Since our goal is to predict attributes of interest y_i and obtain a unique representation from a pruned image set $\hat{D}_i$ across districts (i.e., $n = 230$ administrative districts), we aimed to produce a dimension size v_i smaller than the number of districts n to avoid overfitting. We implemented a principal component analysis (PCA) to reduce the dimensions of the embedded features v_i, which appears in the center of Figure 5.

Presenting the Embedded Spatial Statistics

This final step addresses the challenge arising from the varying input size in which a different number of image tiles define districts. Previous studies in a different domain have attempted to address such arbitrary input length problems via preprocessing techniques, such as adding sequence padding or recurrent neural network-based learning (Yang et al., 2016; Hochreiter and Schmidhuber, 1997). However, these methods cannot resolve the substantial differences in input lengths typical in demographic research. The smallest district could be covered by fewer than ten image tiles, whereas the largest district requires more than hundreds of tiles, resulting in orders of magnitude difference.

We present a technique to summarize any length of image features into a fixed set of vectors. Let g be the composition of the fine tuned feature extractor and k $(1 \leq k \leq 10)$ be the resulting principal components. All images d_j^i in $\hat{D}_i$ are transformed to $v_j' \in \mathbf{R}^k$ by g. Let the matrix of the final embedded vectors from district i be $R_i \in \mathbf{R}^{n_i \times k}$.

To produce a fixed-length embedding from vast geographic areas, we propose to utilize the following descriptive statistics: (i) the mean μ, (ii) the standard deviation σ, (iii) the number of satellite images of a district n, and (iv) Pearson's correlation of the dimensionally reduced features ρ. These four quantities are fundamental *embedded spatial statistics* capturing the observation that satellite images of areas with geoproximity exhibit similar traits. Descriptive statistics represent data by central tendency (mean, median, and mode), dispersion (variance, standard deviation, and skewness), and association (chi-square and correlation). The proposed quantities are descriptive

statistics representing satellite images that belong to the same district.

Finally, cross-products of features were added to consider interactions to enrich the information regarding unknown embedded space distributions. These complete sets of features were learned per district i, as illustrated in the bottom part of Figure 5 and became a fixed-sized representation $\mathbf{r}_i$. To predict the y_i value for district i, we used $\mathbf{r}_i$ to fit a regressor.

4.1.2. Data

This study utilizes the following data: regional-level demographics and high-resolution World Imagery satellite images. We chose South Korea as a representative developed country for training the model. Then, among all available satellite images of South Korea, we further identified those in which at least three vertices of an image tile belong to the polygon representing the boundaries of each district. This heuristic is simple but reasonable for addressing various polygon shapes. In total, 96,131 satellite images (256×256 pixels) of 230 South Korean districts were collected this way. The utilization of all image tiles per district distinguishes our work from those of others, c.f., previous studies used a fixed set of satellite images. For example, a seminal study conducted in African countries used 100 randomly chosen image tiles over $10x10\ km^2$ areas (Jean et al., 2016).

4.1.3. Results

Performance Evaluation and Ablation Study

We conduct a set of experiments. The first evaluation takes advantage of the population demographics by dividing these data into a training set and a test set in an 80–20 ratio. 4-fold cross-validation is applied to the training data set to tune the model's hyperparameters, such as the PCA dimensions and the regularization term in the cost function.

We implemented nine baselines to evaluate. Nightlight uses the districts' total light intensity from nighttime satellite imagery to predict economic scales (Bagan and Yam-

agata, 2015). A regressor was built and trained to obtain the sum of nightlights in each district. Then, Auto-Encoder extracts compact features as step-2. An autoencoder is an unsupervised deep learning algorithm that does not need any label information. The model aims to learn an approximate identity function to construct an output similar to the input while limiting the number of hidden layers. No-Proxy is identical to the proposed model but lacks any knowledge transfer from the proxy dataset. This model was pretrained only with the ImageNet dataset and, hence, can demonstrate the value of the custom dataset.

To verify the effectiveness of READ compared to a well-known model (Xie et al., 2016), we trained JMOP (Jean Model with Our Proxy) which is a combination of two models. First, we use a proxy that predicts rural, urban, and inhabited classes in the same method of READ. Then, we summarize the features and use them to predict with an identical set of model (Xie et al., 2016). Finally, SOTA is the best known grid-based approach for population density prediction (Facebook, 2019). The implementation details of this model are not published, but the prediction results on each arc second block (approximately $30 \times 30\ m^2$) are shared online. We could aggregate the published grid-level data across districts and regress such data with ground truth statistics. The four remaining baselines are ablation studies that remove each feature from READ.

All models were trained with an 80–20 train-test ratios and 4-fold cross-validation. XGBoost (Chen and Guestrin, 2016) was used to enhance prediction accuracy. The models were evaluated 20 times with a randomly split dataset. Table 1 reports the mean and standard deviation of the predictions. READ outperforms all of the nine baselines in both the R-squared (R^2) and mean squared error (MSE) values. Our model even outperforms the current state-of-the-art (SOTA) approach, which is (Facebook, 2019). We find that transfer learning from the custom land cover dataset helps produce a more meaningful embedded, by distilling knowledge associated with urban and rural classifications. The increased prediction quality demonstrates this finding against two models: No-Proxy and Auto-Encoder.

Table 1: Model Prediction Performance Results and Ablation Study

Model	MSE	R-Squared
Nightlight	0.4254±0.0664	0.6133±0.0635
Auto-Encoder	1.6242±0.3445	0.6347±0.0823
No-Proxy	0.2800±0.1118	0.7359±0.1117
JMOP	0.4448±0.0998	0.8985±0.0253
SOTA	-	**0.9231**
READ w/o μ	0.2612±0.0632	0.9429±0.0155
READ w/o ρ	0.2165±0.0596	0.9527±0.0140
READ w/o n	0.1921±0.0471	0.9579±0.0119
READ w/o σ	0.1902±0.0592	0.9586±0.0130
READ	**0.1761±0.0383**	**0.9617±0.0090**

Note: The performance tests were made for prediction of population density.

Furthermore, the quality gain over JMOP indicates that the summarizing technique of READ contributes massively to the performance gain. We perform ablation study to examine the importance of our model components. Ablation study refers to the analysis that removes a particular component of the model, and investigates how that affects the overall performance. The ablation study shows that removing any of the descriptive statistics lowered the performance, indicating that n, μ, ρ, and σ all make a meaningful contribution.

Evaluation Over Broader Scales and Countries

The final evaluation reports predictions of a set of socioeconomic measures by READ. All values are log-scaled, and XGBoost is used. The average R^2 of 20 trials of prediction of the study area is shown in Table 2. The second column shows precise predictions of READ applied to South Korea to predict the population density and its subclass divided by age groups ($R^2 > 0.95$). Predictions on income per capita are 0.76 for R^2. Finally, two demographics in the household category show an extreme difference in their pre-

diction quality: While the household count per square kilometer reports the highest R^2 of 0.9664, the average household size reports the lowest R^2, i.e., 0.6181, among the socioeconomic measures.

Table 2: Prediction Performance for South Korea and Vietnam

Target variable	**South Korea**	**Vietnam**
Population density	**0.9617**	**0.8863**
Population density by age *0-14*	0.9520	0.8756
Population density by age *15-29*	0.9570	0.8791
Population density by age *30-44*	0.9575	0.8881
Population density by age *45-59*	0.9624	0.8804
Population density by age *60+*	0.9654	0.8731
Household count	0.9664	0.8896
Household size	0.6181	0.4460
Income per capita	0.7603	0.6822

Note: The highest R^2 value for each country is highlighted in bold.

The high prediction capability of READ may be due to the custom dataset, which was built from the same country (see step-1 in Figure 5). To test its applicability to another country, Vietnam, we gathered a total of 226,305 satellite images along with its socioeconomic measure data. Then, we applied the model learned from South Korea to predict the socioeconomic measures of Vietnam. Table 2 shows the prediction results. Predictions on population densities show surprisingly high R^2 values, averaging at around 0.88. This is despite the model being trained solely on data from a different country.

The results from the above exercise demonstrate that the learned spatial representation of READ successfully captures general indicators of socioeconomic measures that extend beyond a single country use. However, it is plausible that the strikingly high prediction performance across South Korean and Vietnam is because both countries exhibit similar pathways in economic growth and demographic transition (McNicoll,

2006).

4.2. Measuring Economic Development Under Absence of Ground-truth Data[5]

To overcome the lack of economic data to be used as ground-truth, we developed a deep learning model that learns from high-resolution satellite images to *rank relative scores* of economic development without any labeled data. Specifically, we apply metric learning to score *relative* economic activities, which avoids the use of ground-truth economic data. Metric learning aims to define a task-specific metrics in a supervised manner from a given dataset. Our metric learning algorithm learns to score satellite images for the relative level of economic development measured by urbanization. Our deep neural network first clusters images based on visual features and then defines ordered and paired sets of clusters, i.e., a partial order graph (POG). The POG, an input to the metric learning, contains the information on whether a specific cluster is more urbanized than each of the other clusters. Trained with the constructed POG, our algorithm assigns a score to each satellite image in the final step.

The POG is an essential element in our approach, addressing the limitations of the existing methods. First, since a POG can be generated either by readily available data or by light human annotation, our model can be applied to the cases without labeled data. That is, our model can be used both for developing economies where labeled data is limited and for developed economies where grid-level census data are not gathered frequently. Second, since the POG is an interpretable input to our deep learning algorithm, it helps us to understand the final scores that the algorithm produces. We believe our approach makes one step toward resolving the Black Box problem.

Our model operates in three stages. The first stage (siCluster) uses an entire collection of satellite images of a target country and clusters them by a deep learning-based unsupervised learning and transfer learning. siCluster uses labels for the general land

[5]This subsection is adapted from our work Han et al. (2020b).

cover types, such as rural, urban, and uninhabited. The second stage (siPog) builds a POG of the clusters from siCluster. The order of a POG captures the relative level of economic development, for which we use urbanization as a comprehensive proxy, following the economics literature (Henderson, 2003). Two different methods to generate a POG are suggested: the clusters are ordered either by humans (*human-guided*) or by data such as population density or nightlight intensity (*data-guided*). Lastly, the final stage (siScore) uses the POG from siPog to assign a differentiable score, via a CNN-based model.

The proposed computational framework to measure sub-district level economic development from satellite imagery without the guide of any partial ground-truth data is novel and shows remarkable performance gain over existing baselines. Codes and implementation details are made available at the project repository.[6]

4.2.1. Model Overview

> **Problem definition:** Let $\mathcal{I} = \{\mathbf{x}_1, \mathbf{x}_2, \ldots, \mathbf{x}_n\}$ be the set of satellite images for a given area. The main goal of the proposed model f is to compute a score $\hat{y}_i$ for each image $\mathbf{x}_i$ (i.e., $\hat{y}_i = f(\mathbf{x}_i)$) that well represents the economic development level y_i. We assume ground truth values of y_i are unknown at the training phase.

As a solution, we propose a weakly-supervised method to estimate relative scores that highly correlate with the target variable y_i, rather than predicting its absolute values directly. The method consists of three steps, which are described in Figure 7.

4.2.2. Clustering Satellite Imagery with siCluster

To generate scores that represent the urbanization level, one needs to know what kinds of human activities capture such values. For distinguishing various human activities

[6] https://github.com/dscig/urban_score

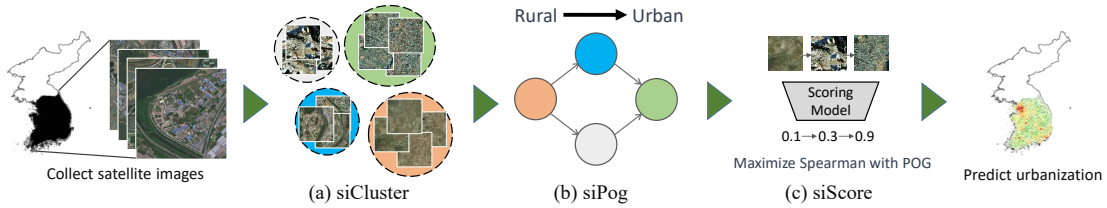

Figure 7: The Model Overview

Note: The overall architecture of the proposed model, composed of (a) siCluster for clustering satellite images, (b) siPog for generating partial order graph (POG), and (c) siScore for training the scoring model with POG.

from satellite imagery, we adopt DeepCluster (Caron et al., 2018), the deep learning-based clustering that can efficiently handle the curse of dimensionality problem via hierarchical architectures (Goodfellow et al., 2016; Krizhevsky et al., 2012).

DeepCluster has two limitations. One is the initial randomness; the model is affected by the initial weights that can propagate through the training process. Another is the lack of consistency in the class assignment; the model relies on the pseudo-labels generated from its k-means clustering, subject to noise in data. As a result, DeepCluster is not directly applicable to our problem, and the satellite grids are grouped according to trivial traits such as RGB patterns (Caron et al., 2018; Ji et al., 2019). Our clustering algorithm, siCluster, builds upon DeepCluster with two new improvements.

Improvement #1 from transfer learning: To give a good initial point for the encoder, we constructed a labeled dataset for transfer learning that includes one thousand satellite images with three labels: urban, rural, and uninhabited. We then adopted a semi-supervised learning technique to train the classifier over the small set of labels and massive amounts of unlabeled data. The Mean Teacher (Tarvainen and Valpola, 2017) model, which penalizes the inconsistent predictions between the teacher and student, is used.

Improvement #2 from consistency preserving: We added new loss terms to prevent the model from learning trivial features. Suppose a given satellite grid $\mathbf{x}_i$ and its corresponding encoded vector $\mathbf{v}_i$, i.e., $\mathbf{v}_i = h_W(\mathbf{x}_i)$. We then augment $\mathbf{x}_i$ via common

techniques such as rotation, gray-scale, and flipping that do not deform the original visual context. Let us call the augmented versions $\hat{\mathbf{x}}_i$. Then, the distance between $\mathbf{x}_i$ and its augmentations $\hat{\mathbf{x}}_i$ in the embedding space should be close enough, compared with the distance between $\mathbf{x}_i$ to other data points. We define the *consistency preserving loss* to represent this invariant feature characteristic against data augmentation in the embedding space. siCluster is trained by jointly optimizing the negative log-likelihood loss and reducing the Euclidean distance between the input and its augmentations on embedding space (Eq. 1).

$$L_{ecp} = \frac{1}{|\mathcal{B}|} \sum_{i \in \mathcal{B}} || \, h_W(\mathbf{x}_i) - h_W(\hat{\mathbf{x}}_i) \, ||_2 \tag{1}$$

4.2.3. Constructing Partial Order Graph with siPog

Images within each cluster share similar visual contexts that likely represent a similar level of economic development. The second step of the algorithm aims at ordering these identified clusters. The partial order graph (POG) is an efficient representation showing the order across different clusters while ignoring any within-cluster difference. We generated a POG in the order of economic development. Here, development refers to an economic transition from agriculture to manufacturing and service industries, which tend to cluster in more urbanized areas (Henderson, 2003). When two clusters showed a similar level of development, they were placed at the same level without any strict ordering between them, as illustrated in Figure Figure 7(b). Below are two strategies of siPog.

Human-guided Method

We first considered the human-in-the-loop design and asked human annotators to sort clusters manually. Both experts and laypeople participated in this ordering task. Annotators compared clusters and identified relative orders of clusters by examining the provided grid images. Clusters were ordered and connected as a graph by their presumed economic development level. Cluster pairs whose development levels were

judged to be indifferent were placed at the same level within the POG. The strength of this method is its lower cost than the full comparison of images.

Data-guided Method

POG can also be generated without human guidance. While grid-level demographics are costly to obtain, there are ample resources that can be used as a proxy, such as Internet search results. Proxy data are aggregated at a high-level (e.g., city or province) or are not accurate. Below we demonstrate one example, *nightlight luminosity*.

Nightlight luminosity is the light intensity measured in nighttime satellite imagery. This publicly free data is only available at low resolution. We first extrapolate the nighttime images to match the size of the daytime satellite grids. Once we identify all the extrapolated nighttime grids corresponding to each cluster, nightlight intensity was averaged for each cluster. We perform a two-sample t-test with a threshold 0.01 to detect any significant intensity difference between every two clusters and consequently create an edge between them if two clusters are sufficiently comparable.

4.2.4. Computing Scores with siScore

Now given the relative orders of clusters in the POG, the next task is to assign a score between 0 and 1 to every cluster using the CNN-based scoring model f. The model automatically detects which features of satellite imagery (belonging to clusters) determine the urbanization score via supervised learning. We adopt the list-wise metric learning method with our unique structures for the scoring model, siScore. During training, we limit the range of values of the scoring model from 0 to 1 by clamping smaller or larger values.

List-wise Metric Learning

The only knowledge from POG is the orders of clusters, but not the orders of individuals images. The third step, siScore, use the POG structure in learning scores of every satellite grid in the following way. We first extract every ordered path from the POG. After choos-

ing one path from them, an equal batch size of n_s images are sampled from each cluster C_k along the selected path. Since the selected path is already ordered, the cluster's actual rank in the path is aligned. The scoring model f trains to match two ranks: generated rank from the model score and actual rank based on POG. The Spearman correlation evaluates how well given two variables are related as a monotonic function in terms of measuring rank correlation. Accordingly, we calculate and maximize the Spearman correlation of the estimated ranks against the actual rank to train the model.

The Spearman correlation is not differentiable and thereby unsuitable due to the back-propagation nature of deep learning. Based on recent advances in computing ranking losses, we use a simple approximation method suggested in Engilberge et al. (2019) to mimic the sorting algorithm and make the algorithm differentiable to use the Spearman correlation as a loss directly.

Variance Regularization

Finally, we added a loss to regularize each cluster's score distribution to satisfy the small score variance within each cluster. With small variances in score distributions, the overlapping part between two adjacent score distributions, where the flipped results are brought, would be reduced. The average variance of score distributions of every cluster in the selected path P_j is minimized as a regularization loss:

$$L_{var} = \frac{1}{|P_j|} \sum_{C_i \in P_j} Var(f(\mathbf{X}_{C_i})), \tag{2}$$

where $\mathbf{X}_{C_i}$ indicates the batch images in cluster C_i and Var denotes the function that calculates the variance of the given score list.

Finally, loss for maximizing Spearman correlation (L_s) and loss for variance regularization (L_{var}) are concurrently optimized to train siScore with the weight parameter α as in Eq. 3.

$$L_{score} = L_s + \alpha \times L_{var} \tag{3}$$

4.2.5. Data

Satellite Imagery

We use the World Imagery dataset from ESRI in the zoom level (Z) 15 with $4.7m$-resolution, which can distinguish individual buildings as well as other artifacts such as roads. Each tile contains three spectral bands (RGB), and the images are cloud-free for most of the area. We consider data from three countries: South Korea, Malawi, and Vietnam, where images are from between 2015 and 2017. Nighttime luminosity is available for public use from the NASA Earth Observing System Data and Information System with the best resolution at $Z = 9$ due to its blurring effect.

Ground-truth Dataset

We use two grid-level ground truth labels: Facebook population and gross floor area. Since the unit area of the Facebook population is smaller than our grid size, we sum up the estimated population density of each unit located inside the grid for evaluation. The gross floor area is computed from GIS data and detailed information on building shapefiles from the official data released in South Korea.

4.2.6. Model Evaluation

We evaluated our model performance on the South Korea dataset. In South Korea, the optimal number of clusters was found to be 21 based on grid search. The POG with discovered clusters was generated as follows. *Human-guided* method involved annotations from five experts and five locals, where both the average and the maximum performance are reported. For data-guided POG, we utilized grid-level nightlight intensity data (*Nightlight-guided*). Table 3 reports the correlation values between the estimated economic development and two kinds of ground truth labels: Gross Floor Area and Population. Both Spearman and Pearson correlations were calculated on the log-scaled ground truth values. All models produced scores of solid correlation (i.e., above 0.7) with ground truth labels, even when such information was not available

Table 3: Model Performance Test Results for South Korea

	Method	Gross Floor Area		Population	
		Spearman	Pearson	Spearman	Pearson
A	Human-guided (Avg)	0.825	0.787	0.764	0.766
	Human-guided (Max)	**0.851**	0.800	**0.795**	0.778
	Nightlight-guided	0.846	0.801	0.794	0.789
B	Nightlight-only	0.664	0.655	0.728	0.731
	Pairwise (Human)	0.651	0.610	0.300	0.302
C	K-means	0.434	0.587	0.451	0.557
	DeepCluster	0.618	0.559	0.532	0.551
D	Triplet (POG)	0.807	0.754	0.768	0.726
	Pairwise (POG)	0.825	0.759	0.767	0.739
	w/o Score model	0.737	0.675	0.678	0.673

A : Our model, B : Baselines, C : siCluster ablation, D : siScore ablation

Note: Two grid-level statistics, gross floor area and population, are used for evaluation criteria.

during training. The best performance comes from the human-guided model, reaching 0.851 and 0.795 in Spearman correlations.

Seven baselines were implemented for comparison, which used ResNet-18 as the backbone network. *(1) Nightlight-only* uses the nightlight intensity for measuring economic development. We also experimented with human-annotated labels *(2) Pairwise (Human)* that indicated the relative rank of four thousand random image pairs. Three annotators with domain knowledge of target countries were asked to choose which image in pair showed higher economic development, and their decisions were aggregated. Training then used the pairwise loss. This model is a simple method that directly learns from the human-annotated orderings. These baselines are less effective than our models.

The next two baselines were ablations for siCluster. We replaced this module by the conventional *(3) K-means* clustering algorithm and the original *(4) DeepCluster* algorithm. The remaining three were ablations for siScore. The labels for *(5) Triplet (POG)* and *(6) Pairwise (POG)* were generated by an identical POG instead of human annota-

tion. When generating labels from the POG, cluster pairs were randomly selected, and images from each cluster formed pairs. The order of chosen clusters was considered as a label for these pairs. Triplet labels included anchor, positive, and negative samples. The model was trained to generate a similar score between the anchor and positive data points while producing different and order-preserving scores between the anchor and negative data points. We also proposed baseline *(7) without the score model*, which gives a scalar value that preserves the orders of POG to each cluster instead of a deep learning-based score model. Nightlight-guided POG is used for these baselines.

4.2.7. Application to Developing Economies

We conducted additional experiments on two developing economies, Malawi and Vietnam, with a total of 64,303 and 226,305 satellite images for each country, respectively. All models were trained in the same manner as mentioned earlier, except for the cluster count n_t in siCluster. The optimal n_t was found to be 7 for Malawi and 11 for Vietnam based on grid search.

Figure 8 compares the performance of the models, evaluated by the grid-level Facebook population data (Facebook, 2020). Our model repeatedly outperforms the conventional nightlight model for developing economies. In the case of Malawi (i.e., the poorer of the two), our models improve the correlation to the Facebook data from 'weak' to 'strong'. The advantage of our model is attributed to the use of daytime imagery, which overcomes the light saturation effect in nighttime satellite images. Moreover, nighttime satellite imagery is known to be erroneous for areas of extreme poverty since the light intensity is very low and varies little in these areas (Jean et al., 2016).

Next, Figure 9 shows the transferability of the model when it is trained on one country's data and tested on another country's data. As one might expect, training and testing a model in the same country (i.e., the diagonal line) shows the highest performance in most cases. South Korea showed consistently above 0.6 Spearman correlation even when the model was trained on Malawi or Vietnam data, for all Human and Nightlight

Figure 8: Results for Malawi and Vietnam

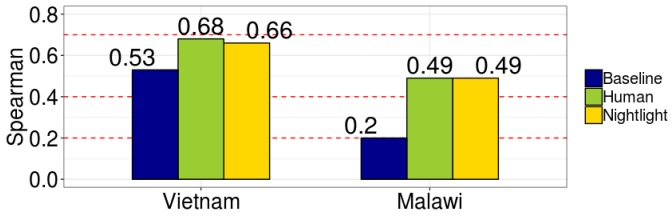

Note: Two models (Human and Nightlight) are compared against the conventional nightlight model (Baseline). The red lines indicate the boundaries for 'weak,' 'moderate,' 'strong,' and 'very strong' correlations from the bottom.

Figure 9: Cross-country Performance Test of a Trained Model

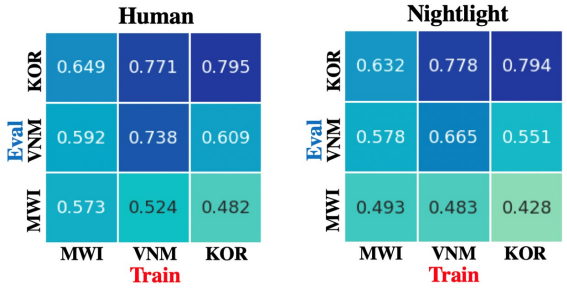

Note: Spearman correlation with ground-truth population for models that are trained in one country and evaluated in another country. Results from two designs of POG generation are visualized respectively.

strategies. We speculate that a comparatively broad spectrum of urbanized patterns in South Korea contributes to this result. This may be linked to the fact that South Korea data required the highest number of clusters (21) compared to the other two (7 and 11), again likely because there were many more distinctive grids with the sufficient numbers of images in each cluster, showing vastly broad economic spectrum. In contrast, the poorest economy (i.e., Malawi) images may contain smaller variations across the grid images.

5. Conclusions and Our Future Agenda

5.1. Model Improvement

Still, our model has much room for improvements. In the proposed siScore model, scores generated from the model cannot be summed due to its lack of linearity. That is, the model cannot evaluate relative scores for the arbitrarily sized area beyond the fixed grid-level satellite imagery. If the generated score from the model follows a logarithmic scale, simply summing the scores of satellite images would result in the wrong evaluation. We are currently working on introducing the mixup techniques (Zhang et al., 2017) to guarantee the linearity. Moreover, in order to verify our model's applicability to various countries and generalizability to different economic and demographic contexts, we are preparing for additional experiments on sub-Saharan countries where we expect immense potential benefits from economic data collection driven by machine learning and satellite imagery. Along with model improvements, we also plan to investigate whether the model's performance is sensitive to various design choices, including the zoom level of satellite images, construction of POG, and tunable parameters.

5.2. Validation of Proxy Measures Produced by Satellite Imagery

Another important future agenda of using proxy measures produced by satellite imagery is validation of these measures. Which aspect of economic activity do these proxies capture? For example, economic variables using night light data have a obvious limitation that it only shed light on activities happening at night. While day time satellite images can overcome this limitation, they may not capture economic activities taking place inside of buildings. Is our proxy variables related to production, asset, or consumption? So far, there are few systematic studies investigating how we can interpret proxies produced by remote sensing data. In future research, we plan to identify elements of economic activity strongly associated with our proxies. Establishing the validity of proxy measures generated by satellite imagery is crucial for acceptance of these remote-sensing data as credible measures of economic activity by social scientists.

5.3. Alternative Measure for Regional Inequality

Measuring inequality is challenging. For example, one of the most commonly used inequality measures, the Gini Index, requires reliable information about the citizens' income in a country. In many countries, especially LDCs, official statistics on income are often inaccurate and does not reflect sizable informal economic activities. For example, in sub-Saharan Africa and Latin America, the informal economy accounts for almost 40% of GDP during 2010-2014 (Allard, 2017). Also, authoritarian regimes may have some incentives to inflate their GDP and to understate inequality (Martinez 2019).

It may be possible to generate a remote-sensing data-based Gini index by generating alternative measures of income or economic activity using satellite images through our proposed machine learning methods. Besides, we can augment official income data with our satellite image-based income proxies to reduce measurement errors to generate a revised Gini Index. Our methods can also provide sub-national measures of inequality, which may be of even greater interest to policymakers.

More accurate measures of inequality can be useful for policy targeting. The current COVID-19 pandemic reminded us of the importance of prompt policy responses to those in need faced with adverse shocks. Targeting individuals or regions requires up-to-date information. However, official statistics often take years to be published. Even in South Korea, a relatively more affluent country in the world, the most recent year of provincial-level gross regional domestic product available is 2018. Remote sensing data combined with the application of machine learning methods not only contribute to social scientists and policymakers searching for systematic data on economic activities but also equip policymakers with valuable information to formulate policies aimed to remedy inequality and economic distress.

5.4. Application to North Korean Economy

We have scarce information about North Korea's economy and how the highly centralized, planned economy works. Despite the importance of understanding economic incentives and resource allocation in both the public and private sectors of the economy, most information coming out of the country remains mostly unconfirmed. Notably, North Korea does not publish or disseminate any official statistics on their economy. Moreover, economic activity in the countryside, where 90 percent of the population resides, is deliberately out of sight of the international community. For instance, visitors are required to stay only in the capital city and are always under surveillance. This poses a crucial problem for the international community, mainly when a consistent collection of economic data is essential for understanding North Korea's transition economy and its foreign policies. Thus, there are potentially substantial benefits for using deep learning to predict socioeconomic patterns and trends of North Korea. Below we broadly discuss several research questions that we intend to explore in future studies using machine learning and satellite imagery.

Our first question is how significant events, such as regime change, affect economic development in a highly centralized, planned economy. We plan to focus on specific significant events that had likely influenced social and economic policies. One prominent event involved a change in leadership after the sudden death of Kim Jong-il on December 17, 2011. Because of the highly centralized power structure in North Korea's political system, a change in leadership can induce significant shifts in resource allocation across industries and regions and cause changes to economic development policies. For instance, multiple sources reported that after coming to power, Kim Jong-un announced a market reform policy, known as the May 31 measures of 2014. The reform includes partial decollectivization of farms and the privatization of manufacturing firms (Gray and Lee, 2017). Our empirical approach is to conduct an event study analysis to assess how market reforms affected North Korea's urban and rural economic development, where we obtain economic measures through satellite images.

A related question that we seek to explore is how local market institutions affect economic activities and urban expansion. This is based on the observation that since the late 1990s, large farmers' markets (known as Jangmadang) have been set up across the country, where vendors sell a wide variety of products, including rice, vegetables, alcohol, clothing, cosmetics, and electronics (Park, 2009; Silberstein, 2015; Choe, 2017). Before the establishment of Jangmadang, the economy relied on a public distribution system, and private transactions of food and services were strictly prohibited. The economic reform in 2002 recognized Jangmadang as a place where private market transactions are legal, and the reform in 2014 further encouraged market activity by incentivizing entrepreneurs and companies to engage in market trade. These policy reforms are in many aspects similar to those introduced in China's market reform in the late 1970s and Vietnam's Doi Moi policy reform in the mid-1980s. We have already identified locations of local markets in North Korea. Combining this information with machine-learning predictions on economic activities, we can analyze the relationship between market institutions and economic growth.

Since launching its first nuclear weapons test in 2006, the United Nations Security Council has passed nearly a dozen sanctions against the country (Davenport, 2016). Individual countries, including the US, Japan, South Korea, and the European Union, have also imposed a series of sanctions against North Korea. These sanctions mainly restrict North Korea's military and economic sectors by prohibiting military supplies, exporting raw minerals, and importing crude oil and refined petroleum products. Proponents of tighter sanctions argue that these sanctions pressure the central government to abandon its nuclear program in exchange for economic benefits that could potentially invigorate its impoverished economy (Haggard and Noland, 2010). On the other hand, Lee (2018) uses nightlight luminosity data of North Korea to suggest that international sanctions increased regional inequality. We plan to explore this question using high-resolution daytime satellite images, which can potentially avoid the well-known issue of nightlight luminosity data showing minimal variation in rural areas of

developing countries.

5.5. Application to the Least Developed Countries

Finally, we plan to apply our approach to collect economic data in Least Developed Countries (LDCs) in Sub-Saharan Africa and Asia. This is because collecting high-quality socioeconomic data is extremely costly and challenging for countries with poor infrastructure. According to the United Nations, a country is classified as LDC if it has low Gross National Income, low on human development indicators (nutrition, health, and education), and economically vulnerable. In Asia alone, there are nine LDCs: Afghanistan, Bangladesh, Bhutan, Cambodia, East Timor, Laos, Myanmar, Nepal, Yemen. With accurate measurements of economic and living conditions, government agencies and policymakers can effectively fight poverty and foster economic development.

References

Allard, Céline, "3. The Informal Economy in Sub-Saharan Africa," in "Regional Economic Outlook, April 2017, Sub-Saharan Africa," International Monetary Fund, 2017.

Bagan, Hasi and Yoshiki Yamagata, "Analysis of urban growth and estimating population density using satellite images of nighttime lights and land-use and population data," *GIScience & Remote Sensing*, 2015, *52* (6), 765–780.

Baragwanath, Kathryn, Ran Goldblatt, Gordon Hanson, and Amit K Khandelwal, "Detecting urban markets with satellite imagery: An application to India," *Journal of Urban Economics*, 2019, pp. 103–173.

Bharti, Nita, Andrew J Tatem, Matthew J Ferrari, Rebecca F Grais, Ali Djibo, and Bryan T Grenfell, "Explaining seasonal fluctuations of measles in Niger using nighttime lights imagery," *Science*, 2011, *334* (6061), 1424–1427.

Butler, Declan, "AI summit aims to help world's poorest," *Nature*, 2017, *546* (7657).

Caron, Mathilde, Piotr Bojanowski, Armand Joulin, and Matthijs Douze, "Deep clustering for unsupervised learning of visual features," *proc. of the ECCV*, 2018, pp. 132–149.

Castelvecchi, Davide, "Can we open the black box of AI?," *Nature News*, 2016, *538* (7623), 20.

Chen, Liang-Chieh, Yukun Zhu, George Papandreou, Florian Schroff, and Hartwig Adam, "Encoder-decoder with atrous separable convolution for semantic image segmentation," *proc. of the ECCV*, 2018, pp. 801–818.

Chen, Tianqi and Carlos Guestrin, "Xgboost: A scalable tree boosting system," *proc. of the ACM SIGKDD*, 2016, pp. 785–794.

Chen, Xi and William D Nordhaus, "Using luminosity data as a proxy for economic statistics," *PNAS*, 2011, *108* (21), 8589–8594.

Chen, Xueyun, Shiming Xiang, Cheng-Lin Liu, and Chun-Hong Pan, "Vehicle detection in satellite images by hybrid deep convolutional neural networks," *IEEE Geoscience and Remote Sensing Letters*, 2014, *11* (10), 1797–1801.

Choe, Sang-Hun, "As Economy Grows, North Korea's Grip on Society is Tested," 2017. The New York Times.

Chui, Michael, Martin Harryson, James Manyika, Roger Roberts, Rita Chung, Ashley van Heteren, and Pieter Nel, "Notes from the AI frontier: Applying AI for social good," *McKinsey Global Institute*, 2018.

Daudt, Rodrigo Caye, Bertr Le Saux, Alexandre Boulch, and Yann Gousseau, "Urban change detection for multispectral earth observation using convolutional neural networks," *IGARSS 2018-2018 IEEE International Geoscience and Remote Sensing Symposium*, 2018, pp. 2115–2118.

Davenport, Kelsey, "UN Security Council Resolutions on North Korea," 2016. Washington, D.C., USA: Arms Control Association.

Deng, Jia, Wei Dong, Richard Socher, Li-Jia Li, Kai Li, and Li Fei-Fei, "Imagenet: A large-scale hierarchical image database," *2009 IEEE conference on computer vision and pattern recognition*, 2009, pp. 248–255.

Dingel, Jonathan I, Antonio Miscio, and Donald R Davis, "Cities, lights, and skills in developing economies," *Journal of Urban Economics*, 2019, pp. 103–174.

Donaldson, Dave and Adam Storeygard, "The view from above: Applications of satellite data in economics," *Journal of Economic Perspectives*, 2016, *30* (4), 171–98.

Doxsey-Whitfield, Erin, Kytt MacManus, Susana B Adamo, Linda Pistolesi, John Squires, Olena Borkovska, and Sandra R Baptista, "Taking advantage of the improved availability of census data: a first look at the gridded population of the world, version 4," *Papers in Applied Geography*, 2015, *1* (3), 226–234.

Engilberge, Martin, Louis Chevallier, Patrick Pérez, and Matthieu Cord, "SoDeep: a Sorting Deep net to learn ranking loss surrogates," *proc. of the IEEE CVPR*, 2019, pp. 10792–10801.

Facebook, *Data for Good Program*, Facebook, 2019. Available at https://data.humdata.org/organization/facebook. Date accessed 05 Sep 2019.

_ , *Data for Good Program*, Facebook, 2020. Available at https://data.humdata.org/

organization/facebook. Date accessed 29 Jan 2020.

Fatehkia, Masoomali, Ridhi Kashyap, and Ingmar Weber, "Using Facebook ad data to track the global digital gender gap," *World Development*, 2018, *107*, 189–209.

Foley, Jonathan A, Ruth DeFries, Gregory P Asner, Carol Barford, Gordon Bonan, Stephen R Carpenter, F Stuart Chapin, Michael T Coe, Gretchen C Daily, Holly K Gibbs et al., "Global consequences of land use," *Science*, 2005, *309* (5734), 570–574.

Goodfellow, Ian, Yoshua Bengio, and Aaron Courville, *Deep learning*, MIT press, 2016.

Google, "AI for Social Good," Available at https://ai.google/social-good/. accessed 28 May 2020.

Gray, Kevin and Jong-Woon Lee, "Following in China's footsteps? The political economy of North Korean reform," *The Pacific Review*, 2017, *30* (1), 51–73.

Guo, Wei, Wen Yang, Haijian Zhang, and Guang Hua, "Geospatial object detection in high resolution satellite images based on multi-scale convolutional neural network," *Remote Sensing*, 2018, *10* (1), 131.

Haggard, Stephan and Marcus Noland, "Sanctioning North Korea: The Political Economy of Denuclearization and Proliferation," *Asian Survey*, 2010, *50* (3), 539–568.

Han, Sungwon, Donghyun Ahn, Hyunji Cha, Jeasurk Yang, Sungwon Park, and Meeyoung Cha, "Lightweight and Robust Representation of Economic Scales from Satellite Imagery," *Forthcoming in Proceedings of the AAAI Conference on Artificial Intelligence*, 2020.

_ , _ , Sungwon Park, Jeasurk Yang, Susang Lee, Jihee Kim, Hyunjoo Yang, Sangyoon Park, and Meeyoung Cha, "Learning to score economic development from satellite imagery," *Proceedings of the ACM SIGKDD Conference on Knowledge Discovery & Data Mining*, 2020.

Henderson, J V, "Urbanization and Economic Development," *Annals of Economics and Finance*, 2003, *4* (2), 275–341.

_ , Adam Storeygard, and David N Weil, "Measuring economic growth from outer space," *American Economic Review*, 2012, *102* (2), 994–1028.

_ , Tim Squires, Adam Storeygard, and David Weil, "The global distribution of economic activity: Nature, history, and the role of trade," *The Quarterly Journal of Economics*, 2018, *133* (1), 357–406.

Hochreiter, Sepp and Jürgen Schmidhuber, "Long short-term memory," *Neural Computation*, 1997, *9* (8), 1735–1780.

Hodler, Roland and Paul A Raschky, "Regional favoritism," *The Quarterly Journal of Economics*, 2014, *129* (2), 995–1033.

Jayachandran, Seema, Joost De Laat, Eric F Lambin, Charlotte Y Stanton, Robin Audy, and Nancy E Thomas, "Cash for carbon: A randomized trial of payments for ecosystem services to reduce deforestation," *Science*, 2017, *357* (6348), 267–273.

Jean, Neal, Marshall Burke, Michael Xie, W Matthew Davis, David B Lobell, and Stefano Ermon, "Combining satellite imagery and machine learning to predict poverty," *Science*, 2016, *353* (6301), 790–794.

Ji, Xu, Joao F Henriques, and Andrea Vedaldi, "Invariant information clustering for unsupervised image classification and segmentation," *proc. of the IEEE ICCV*, 2019, pp. 9865–9874.

Johnston, Kevin, Jay M Ver Hoef, Konstantin Krivoruchko, and Neil Lucas, *Using ArcGIS Geostatistical Analyst*, Vol. 380, Esri Redlands, 2001.

Khan, Salman H, Xuming He, Fatih Porikli, and Mohammed Bennamoun, "Forest change detection in incomplete satellite images with deep neural networks," *IEEE Transactions on Geoscience and Remote Sensing*, 2017, *55* (9), 5407–5423.

Krizhevsky, Alex, Ilya Sutskever, and Geoffrey E Hinton, "Imagenet classification with deep convolutional neural networks," *proc. of the NIPS*, 2012, pp. 1097–1105.

Lee, Yong Suk, "International isolation and regional inequality: Evidence from sanctions on North Korea," *Journal of Urban Economics*, 2018, *103*, 34–51.

Marx, Benjamin, Thomas M Stoker, and Tavneet Suri, "There is no free house: Ethnic patronage in a Kenyan slum," *American Economic Journal: Applied Economics*, 2019, *11* (4), 36–70.

McNicoll, Geoffrey, "Policy Lessons of the East Asian Demographic Transition," *Population and Development Review*, 2006, *32* (1), 1–25.

Michalopoulos, Stelios and Elias Papaioannou, "Pre-colonial ethnic institutions and contemporary African development," *Econometrica*, 2013, *81* (1), 113–152.

_ and _ , "Spatial patterns of development: A meso approach," *Annual Review of Economics*, 2018, *10*, 383–410.

Microsoft, "Using AI for Good with Microsoft AI," Available at https://www.microsoft.com/en-us/ai/ai-for-good. accessed 28 May 2020.

Naik, Nikhil, Scott Duke Kominers, Ramesh Raskar, Edward L Glaeser, and César A Hidalgo, "Computer vision uncovers predictors of physical urban change," *PNAS*, 2017, *114* (29), 7571–7576.

Park, In-Ho, "2008 Top Items in the Jangmadang," 2009. North Korean Economy Watch http://www.nkeconwatch.com.

Pinkovskiy, Maxim, "Growth discontinuities at borders," *Journal of Economic Growth*, 2017, *22* (2), 145–192.

_ and Xavier Sala i Martin, "Lights, camera… income! Illuminating the national accounts-household surveys debate," *The Quarterly Journal of Economics*, 2016, *131* (2), 579–631.

Rama, Daniele, Yelena Mejova, Michele Tizzoni, Kyriaki Kalimeri, and Ingmar Weber, "Facebook Ads as a Demographic Tool to Measure the Urban-Rural Divide," *proc. of The Web Conference 2020*, 2020, p. 327–338.

Sheehan, Evan, Chenlin Meng, Matthew Tan, Burak Uzkent, Neal Jean, Marshall Burke, David Lobell, and Stefano Ermon, "Predicting economic development using geolocated wikipedia articles," *proc. of the ACM SIGKDD*, 2019, pp. 2698–2706.

Silberstein, Benjamin K., "A new defector survey about market trade in North Korea, and what it says (maybe) about Kim Jong-un," 2015. North Korean Economy Watch http://www.nkeconwatch.com.

Storeygard, Adam, "Farther on down the road: transport costs, trade and urban growth

in sub-Saharan Africa," *The Review of Economic Studies*, 2016, *83* (3), 1263–1295.

Tarvainen, Antti and Harri Valpola, "Mean teachers are better role models: Weight-averaged consistency targets improve semi-supervised deep learning results," *proc. of the NIPS*, 2017.

Uzkent, Burak, Evan Sheehan, Chenlin Meng, Zhongyi Tang, Marshall Burke, David Lobell, and Stefano Ermon, "Learning to Interpret Satellite Images using Wikipedia," *proc. of the IJCAI-19*, 2019, pp. 3620–3626.

Wang, Yi-Chen, Benjamin KH Hu, Soe W Myint, Chen-Chieh Feng, Winston TL Chow, and Paul F Passy, "Patterns of land change and their potential impacts on land surface temperature change in Yangon, Myanmar," *Science of the Total Environment*, 2018, *643*, 738–750.

Wang, Yingming, Lijun Wang, Huchuan Lu, and You He, "Segmentation Based Rotated Bounding Boxes Prediction and Image Synthesizing for Object Detection of High Resolution Aerial Images," *Neurocomputing*, 2020, *388*.

Xie, Michael, Neal Jean, Marshall Burke, David Lobell, and Stefano Ermon, "Transfer learning from deep features for remote sensing and poverty mapping," *proc. of the AAAI*, 2016, pp. 3929–3935.

Xie, Yanhua and Qihao Weng, "Updating urban extents with nighttime light imagery by using an object-based thresholding method," *Remote Sensing of Environment*, 2016, *187*, 1–13.

Yang, Zichao, Diyi Yang, Chris Dyer, Xiaodong He, Alex Smola, and Eduard Hovy, "Hierarchical attention networks for document classification," *proc. of the NAACL-HLT*, 2016, pp. 1480–1489.

Yeh, Christopher, Anthony Perez, Anne Driscoll, George Azzari, Zhongyi Tang, David Lobell, Stefano Ermon, and Marshall Burke, "Using publicly available satellite imagery and deep learning to understand economic well-being in Africa," *Nature Communications*, 2020, *11* (1), 1–11.

Zhang, Hongyi, Moustapha Cisse, Yann N Dauphin, and David Lopez-Paz, "Mixup:

Beyond empirical risk minimization," *arXiv preprint arXiv:1710.09412*, 2017.